Inorg. Chem. **2007**, *46*, 2261–2271

Formation of Antiferromagnetically Coupled $C_{60}^{\bullet-}$ and Diamagnetic $(C_{70}^{-})_2$ Dimers in Ionic Complexes of Fullerenes with $(MDABCO^{+})_2 \cdot M^{II}TPP$ (M = Zn, Co, Mn, and Fe) Assemblies

Dmitri V. Konarev,*,†,‡ Salavat S. Khasanov,†,§ Akihiro Otsuka,|| Gunzi Saito,*,† and Rimma N. Lyubovskaya‡

Division of Chemistry, Graduate School of Science, Kyoto University, Sakyo-ku, Kyoto 606-8502, Japan, Institute of Problems of Chemical Physics RAS, Chernogolovka, Moscow region 142432, Russia, Institute of Solid State Physics RAS, Chernogolovka, Moscow region, 142432, Russia, and Research Center for Low Temperature and Materials Sciences, Kyoto University, Sakyo-ku, Kyoto 606-8502, Japan

Received June 20, 2006

A series of ionic multicomponent complexes comprising C_{60} and C_{70} anions and coordinating assemblies of methyldiazabicyclooctane cations with metal tetraphenylporphyrins, $(MDABCO^{+})_2 \cdot M^{II}TPP \cdot (C_{60(70)}^{-})_2 \cdot Sol$. ($C_{60}$, M = Zn (**1**); C_{60}, M = Co (**2**); C_{60}, M = Mn (**3**); C_{60}, M = Fe (**4**); C_{70}, M = Mn (**5**); and C_{70}, M = Fe (**6**)) has been obtained. IR– and UV–vis-NIR spectra of **1**–**6** justified the formation of $C_{60}^{\bullet-}$ in **1**–**4** and single-bonded $(C_{70}^{-})_2$ dimers in **5** and **6**. Co and Mn atoms are six-coordinated in the $(MDABCO^{+})_2 \cdot M^{II}TPP$ units with relatively long M–N bonds of 2.475(2), 2.553(2), and 2.511(3) Å for **2, 3**, and **5**, respectively. Isostructural complexes **2** and **3** contain $C_{60}^{\bullet-}$ zigzag chains separated by the $(MDABCO^{+})_2 \cdot M^{II}TPP$ units, whereas in **5** the layers formed by the $(C_{70}^{-})_2$ dimers alternate with those composed of the $(MDABCO^{+})_2 \cdot Mn^{II}TPP$ units and noncoordinating $MDABCO^{+}$ cations. Negative Weiss constants of –13 (**1**), –2 (**3**), and –2 (**4**) K indicate the antiferromagnetic interaction of spins, which decreases the magnetic moment of the complexes below 70–120 K. The EPR signals of **1** and **4** attributed to $C_{60}^{\bullet-}$ are split into two components at the same temperatures, which broaden and shift to higher and lower magnetic fields with the temperature decrease. Complexes **2** and **3** show single EPR signals with *g*-factors equal to 2.1082 and ~2.4 at 293 K, respectively. These values are mean between those characteristic of $M^{II}TPP$ and $C_{60}^{\bullet-}$, and, consequently, the signals appear due to exchange coupling between these paramagnetic species. The antiferromagnetic ordering of $C_{60}^{\bullet-}$ spins below 70–100 K shifts *g*-factor values closer to those characteristic of individual $M^{II}TPP$ (g = 2.1907 (**2**) and ~4.9 (**3**) at 4 K). In contrast to **1**–**4**, complex **5** shows paramagnetic behavior with Weiss constant close to 0.

Introduction

Compounds of fullerenes with metalloporphyrins form a wide family, which includes covalently linked dyad and triad molecules,[1] coordination dyads,[2] and molecular and ionic donor−acceptor complexes.[3] Some of these compounds show promising photoactive properties.[1,2] Fullerenes are relatively weak acceptors as compared with conventional planar π-acceptors such as tetracyanoethylene and tetracyanoquinodimethane.[4] As a result, most metalloporphyrins cannot reduce fullerenes (even such strong donors as $Mn^{II}TPP$[3c,f] and $Fe^{II}TPP$[3h] (TPP: tetraphenylporphyrin)). It was shown that only $Sn^{II}TTolP$ (TTolP: tetratolylporphyrin) and $Cr^{II}TPP$ reduced C_{60} in the presence of either coordinating ligands or polar solvents.[5] Ionicity of donor−acceptor complexes is an important condition to manifest high conductivity or magnetism.[4] To solve the problem of weak acceptor properties of fullerenes we developed a multicomponent approach, in which strong donors able to reduce C_{60} or cations

* To whom correspondence should be addressed. E-mail: konarev@icp.ac.ru (D.V.K), saito@kuchem.kyoto-u.ac.jp (G.S.).
† Division of Chemistry, Graduate School of Science, Kyoto University.
‡ Institute of Problems of Chemical Physics RAS.
§ Institute of Solid State Physics RAS.
|| Research Center for Low Temperature and Materials Sciences, Kyoto University.

(1) Guldi, D. M. *Chem. Soc. Rev.* **2002**, *31*, 22.
(2) El-Khouly, M. E.; Ito, O.; Smith, P. M.; D'Souza, F. *J. Photochem. Photobiol. C: Rev.* **2004**, *5*, 79.

10.1021/ic0611138 CCC: $37.00
Published on Web 02/22/2007

(D_1^+) are used additionally to neutral metalloporphyrins: (D^+)·{M^{II}porphyrin·(fullerene$^-$)}.[6] This approach can be applied to the porphyrin-fullerene complexes due to that the packing mode of planar porphyrin and spherical fullerene molecules provides large cavities, which can accommodate even bulky counter cations (D^+).[7] The study of [{$Cr^I(C_6H_6)_2^{\bullet+}$}·{$Co^{II}$TPP·(fullerene$^-$)}·$C_6H_4Cl_2$] complexes ($Cr(C_6H_6)_2$: bis(benzene)chromium; fullerenes C_{60} and $C_{60}(CN)_2$) showed that fullerene radical anions are essentially stronger ligands than neutral fullerenes and form coordinating {Co^{II}TPP·(fullerene$^-$)} units with the length of the Co...C(fullerene$^-$) contacts in the 2.28−2.32 Å range.[6a,b] Coordination is realized by σ-type and most probably involves electrons from Co^{II}TPP d_{z^2} and LUMO of C_{60}^-. The resulting {Co^{II}TPP·(fullerene$^-$)} units are diamagnetic.[6] The variation of counter cations affects the stability of {Co^{II}TPP·(C_{60}^-)} units. They are stable up to room temperature in {$(CH_3)_4N^+$}·{Co^{II}TPP·(C_{60}^-)}·(C_6H_5CN)·($C_6H_4Cl_2$),[6c] dissociate above 190 K in (TDAE$^{\bullet+}$)·{Co^{II}TPP·(C_{60}^-)} (TDAE: tetrakis(dimethylamino)ethylene),[6d] and are not formed in {(Cs^+)·(C_6H_5CN)$_{1.64}$·(CH_3CN)}·Co^{II}TPP·($C_{60}^{\bullet-}$)·($C_6H_4Cl_2$)$_{0.36}$.[6c] Recently a similar complex based on cobalt(II) octaethylporphyrin: (TMP^+)·{Co^{II}OEP·(C_{60}^-)}·(C_6H_5CN)$_x$·($C_6H_4Cl_2$)$_{1-x}$ ($x \cong 0.75$) with noncoordinating tetramethylphosphonium cations has been obtained. The σ-bonded diamagnetic {Co^{II}OEP·(C_{60}^-)} units are also found in this complex with the Co···(C_{60}^-) distance of 2.27 Å.[8] All the aforementioned complexes contain only Co^{II}porphyrins, whereas Zn^{II}TPP, Mn^{II}TPP, and Fe^{II}TPP do not form such complexes. This observation was proved by the fact that among these metalloporphyrins only Co^{II}TPP form stable coordination Co−C σ-bonds similar to those observed in alkylcobalamins.[9] Therefore, the formation of such coordination bonds is an important condition for the formation of ionic multicomponent complexes between fullerene anions and metalloporphyrins. Taking into account this fact the multicomponent approach can be developed using coordinating N-containing cations. These cations can coordinate not only to Co(II) porphyrins but also to Zn(II), Fe(II), and Mn(II) porphyrins that allows the range of ionic multicomponent complexes of such type to be essentially expanded. Up to now two complexes with coordinating methyldiazabicyclooctane cations were reported: {($MDABCO^+$)·Co^{II}OEP·(C_{60}^-)}·($C_6H_4Cl_2$)$_{1-x}$·(C_6H_5CN)$_x$ ($x \cong 0.67$)[8] and {($MDABCO^+$)·Co^{II}TMPP}$_2$·(C_{60}^-)$_2$·($C_6H_4Cl_2$)$_{2.5}$·(C_6H_5CN)$_{1.5}$ (TMPP: tetrakis(4-methoxyphenyl)porphyrin).[10] They contain six- and five-coordinated Co^{II}porphyrin units and demonstrate the reversible formation of Co−C(C_{60}^-) coordination bonds with a paramagnetic−diamagnetic transition[8] and the formation of new negatively charged (C_{60}^-)$_2$ dimers bonded by two single bonds.[10]

Chart 1

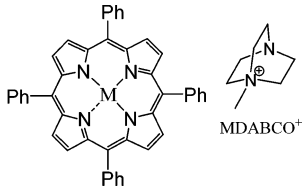

M^{II}TPP (M = Zn, Co, Mn, and Fe)

In this work we present a new series of ionic multicomponent complexes of both fullerenes C_{60} and C_{70} (**1**−**6**) containing new assemblies, in which M^{II}TPP porphyrins (M = Zn, Co, Mn, and Fe, Chart 1) coordinate two $MDABCO^+$ cations (Chart 1), and metal atoms are six-coordinated. Crystal structures of three complexes with both fullerenes C_{60} and C_{70} were studied, and IR, UV−vis-NIR spectra and temperature-dependent EPR and SQUID of **1**−**6** were measured. It was shown that C_{60} complexes **1**−**4** contain monomeric $C_{60}^{\bullet-}$ radical anions, which manifest an antiferromagnetic interaction of spins. C_{70} complexes **5** and **6** contain diamagnetic (C_{70}^-)$_2$ dimers that allow magnetic properties of individual coordinating ($MDABCO^+$)$_2$·M^{II}TPP assemblies (M = Fe, and Mn) to be studied.

Experimental Section

Materials. Zinc(II) tetraphenylporphyrin (ZnTPP), cobalt(II) tetraphenylporphyrin (Co^{II}TPP), manganese(III) tetraphenylporphyrin chloride (Mn^{III}TPPCl), iron(III) tetraphenylporphyrin chloride (Fe^{III}TPPCl), $NaBH_4$, diazabicyclooctane (DABCO), sodium ethanethiolate (CH_3CH_2SNa), and methyl iodide (CH_3I) were purchased from Aldrich. C_{60} of 99.98% purity and C_{70} of 99.0% purity were received from MTR Ltd. Solvents were purified in argon atmosphere. *o*-Dichlorobenzene ($C_6H_4Cl_2$) was distilled over CaH_2 under reduced pressure, benzonitrile (C_6H_5CN) was distilled over Na under reduced pressure, and hexane was distilled over Na/

(3) Olmstead, M. M.; Costa, K.; Maitra, D. A.; Noll, B. C.; Phillips, S. L.; Van Calcar, P. M.; Balch, A. L. *J. Am. Chem. Soc.* **1999**, *121*, 7090. (b) Ishii, T.; Aizawa, N.; Kanehama, R.; Yamashita, M.; Sugiura, K.; Miyasaka, H. *Coord. Chem. Rev.* **2002**, *226*, 113. (c) Yudanova, E. I.; Konarev, D. V.; Gumanov, L. L.; Lyubovskaya, R. N. *Russ. Chem. Bull.* **1999**, *48*, 718. (d) Boyd, P. D. W.; Hodgson, M. C.; Rickard, C. E. F.; Oliver, A. G.; Chaker, L.; Brothers, P. J.; Bolskar, R. D.; Tham, F. S.; Reed, C. A. *J. Am. Chem. Soc.* **1999**, *121*, 10487. (e) Boyd, P. D. W.; Reed, C. A. *Acc. Chem. Res.* **2005**, *38*, 235. (f) Konarev, D. V.; Neretin, I. S.; Slovokhotov, Yu. L.; Yudanova, E. I.; Drichko, N. V.; Shul'ga, Yu. M.; Tarasov, B. P.; Gumanov, L. L.; Batsanov, A. S.; Howard, J. A. K.; Lyubovskaya, R. N. *Chem. Eur. J.* **2001**, *7*, 2605. (g) Konarev, D. V.; Kovalevsky, A. Y.; Li, X.; Neretin, I. S.; Litvinov, A. L.; Drichko, N. V.; Slovokhotov, Yu. L.; Coppens, P.; Lyubovskaya, R. N. *Inorg. Chem.* **2002**, *41*, 3638. (h) Mikami, S.; Sugiura, K.; Asato, E.; Maeda, Y.; Sakat, Y. In *Proceeding of the Conference "The 19th Fullerene General Symposium"*; Kiryu, Japan, July 27−28, 2000; p 40.

(4) Saito, G.; Teramoto, T.; Otsuka, A.; Sugita, Y.; Ban, T.; Kusunoki, M.; Sakaguchi, K. *Synth. Met.* **1994**, *64*, 359.

(5) Pénicaud, A.; Hsu, J.; Reed, C. A.; Koch, A.; Khemani, K.; Allemand, P.-M.; Wudl, F. *J. Am. Chem. Soc.* **1991**, *113*, 6698. (b) Stinchcombe, J.; Pénicaud, A.; Bhyrappa, P.; Boyd, P. D. V.; Reed, C. A. *J. Am. Chem. Soc.* **1993**, *115*, 5212.

(6) Konarev, D. V.; Khasanov, S. S.; Otsuka, A.; Yoshida, Y.; Saito, G. *J. Am. Chem. Soc.* **2002**, *124*, 7648. (b) Konarev, D. V.; Khasanov, S. S.; Otsuka, A.; Yoshida, Y.; Lyubovskaya, R. N.; Saito, G. *Chem. Eur. J.* **2003**, *9*, 3837. (c) Konarev, D. V.; Neretin, I. S.; Saito, G.; Slovokhotov, Yu. L.; Otsuka, A.; Lyubovskaya, R. N. *Eur. J. Inorg. Chem.* **2004**, 1794. (d) Konarev, D. V.; Neretin, I. S.; Saito, G.; Slovokhotov, Yu. L.; Otsuka, A.; Lyubovskaya, R. N. *Dalton Trans.* **2003**, 3886.

(7) Konarev, D. V.; Khasanov, S. S.; Saito, G.; Lyubovskaya. R. N. *J. Porphyrins Phthalocyanines* **2003**, *7*, 801.

(8) Konarev, D. V.; Khasanov, S. S.; Otsuka, A.; Saito, G.; Lyubovskaya, R. N. *Chem. Eur. J.* **2006**, *12*, 5225.

(9) Rossi, M.; Glusker, J. P.; Randaccio, L.; Summers, M. F.; Toscano, P. J.; Marzilli, L. G. *J. Am. Chem. Soc.* **1985**, *107*, 1729.

(10) Konarev, D. V.; Khasanov, S. S.; Otsuka, A.; Saito, G.; Lyubovskaya, R. N. *J. Am. Chem. Soc.* **2006**, *128*, 9292.

Table 1. Data of Elemental Analysis for **1**−**6**

no.	complex	elemental analysis found/calcd C,%	H,%	N,%	Cl,%	M,%
1	$\{(MDABCO)_2{\cdot}ZnTPP\}{\cdot}(C_{60})_2{\cdot}(C_6H_4Cl_2)_{2.5}{\cdot}(C_6H_5CN)_{0.5}$	80.96	2.65	4.17	6.07	
		82.62	2.47	4.18	6.21	2.29
2	$\{(MDABCO)_2{\cdot}CoTPP\}{\cdot}(C_{60})_2{\cdot}(C_6H_4Cl_2)_{4.4}{\cdot}(C_6H_5CN)_{1.6}$	according to X-ray structural analysis				
3	$\{(MDABCO)_2{\cdot}MnTPP\}{\cdot}(C_{60})_2{\cdot}(C_6H_4Cl_2)_{4.2}{\cdot}(C_6H_5CN)_{1.8}$	according to X-ray structural analysis				
4	$\{(MDABCO)_2{\cdot}FeTPP\}{\cdot}(C_{60})_2{\cdot}(C_6H_4Cl_2)_{2.2}{\cdot}(C_6H_5CN)_{0.8}$	82.04	2.77	4.37	5.52	
		83.61	2.30	4.35	5.51	1.97
5	$\{(MDABCO)_2{\cdot}MnTPP\}{\cdot}(MDABCO)_2\{(C_{70})_2\}_2{\cdot}(C_6H_4Cl_2)_6{\cdot}(C_6H_5CN)_5$	according to X-ray structural analysis				
6	$\{(MDABCO)_2{\cdot}FeTPP\}{\cdot}(C_{70})_2{\cdot}(C_6H_4Cl_2)_3$	82.70	2.39	3.61	6.98	
		83.40	2.26	3.69	6.87	1.80

benzophenone. The solvents were degassed and stored in a glove box. All manipulations for the synthesis of air-sensitive **1**−**6** were carried out in a MBraun 150B-G glove box with controlled atmosphere and the content of H_2O and O_2 less than 1 ppm. The crystals were stored in a glove box and sealed in anaerobic conditions in 2 mm quartz tubes for EPR and SQUID measurements under 10^{-5} Torr. KBr pellets for IR− and UV−visible-NIR measurements were prepared in a glove box.

Synthesis. *N*-Methyldiazabicyclooctane iodide (MDABCO·I) was obtained by a dropwise addition of 1 molar equiv of CH_3I (1.11 mL, 0.0178 mol) to DABCO (2 g, 0.0178 mol) dissolved in 60 mL of hexane at stirring. A white crystalline precipitate of MDABCO·I formed during the addition. After 1 h the precipitate was filtered off, washed with 100 mL of hexane, and dried in vacuum during 8 h. MDABCO·I (4.07 g) was obtained with 90% yield and satisfactory elemental analysis.

Iron(II) and manganese(II) tetraphenylporphyrins were obtained by the reduction of M^{III}TPPCl with $NaBH_4$ in anaerobic conditions.[11] About 50 mg of $NaBH_4$ was dissolved in warm ethanol (12 mL), and the solution was cooled down to room temperature and filtered. 500 mg of M^{III}TPPCl was put into the obtained solution (M^{III}TPPCl and M^{II}TPP only slightly dissolved in ethanol). The reduction was carried out during 24 h. The precipitate of reduced metalloporphyrins was filtered off, washed with two portions of ethanol (5 mL), and dried to give Fe^{II}TPP and Mn^{II}TPP with 50−70% yield. The absence of Mn^{III}TPPCl in the samples was proved by visible-NIR spectra. The obtained Mn^{II}TPP can contain coordinating ethanol,[12] whereas Fe^{II}TPP crystallizes from ethanol as a solvent free phase.[13]

The crystals of **1**−**6** were obtained by the following procedure. C_{60} (**1**−**4**) (25 mg, 0.035 mmol), or C_{70} (**5** and **6**) (25 mg, 0.03 mmol), a 10-fold molar excess of CH_3CH_2SNa (30 mg, 0.36 mmol), and a 5-fold molar excess of MDABCO·I (44.5 mg, 0.175 mmol) were stirred in 20 mL of the $C_6H_4Cl_2/C_6H_5CN$ (19:1) mixture for 1 h at 60 °C. C_6H_5CN was added to increase the solubility of CH_3CH_2SNa and MDABCO·I, which are poorly soluble in pure $C_6H_4Cl_2$. During stirring the color of the solution changed from violet characteristic of neutral C_{60} to red-brown. After cooling the solution down to room temperature and filtering, the NIR spectrum was measured to indicate selective reduction of fullerenes to (−1) radical anion state. ZnTPP (**1**), Co^{II}TPP (**2**), Mn^{II}TPP (**3**), Fe^{II}TPP (**4**), Mn^{II}TPP (**5**), and Fe^{II}TPP (**6**) (∼24 mg, 0.035 mmol) were dissolved in the obtained solutions at 60 °C for 1 h, then cooled, and filtered in a 50 mL glass tube of 1.8 cm diameter with a ground glass plug, and 25 mL of hexane was layered over the solution. The diffusion was carried out during 2 months to give crystals of **1**−**6** on the wall of the tube. The solvent was decanted from the crystals, which were then washed with hexane to give black prisms with characteristic blue luster (up to 1 × 1 × 0.5 mm^3 in size) with 50−70% yield.

Careful examination of the crystals of **1** and **3**−**6** under microscope showed that only one phase was harvested in the synthesis. On the contrary, the crystals of **2** were obtained as a mixture of two phases at the least: black large prisms and planar rhombs. We studied the crystal structure of one phase (large prisms) and measured IR−, UV−vis-NIR spectra and temperature-dependent EPR for one single-crystal sample used in the crystal structure determination.

The composition of **1**, **4**, and **6** was determined from the elemental analyses and that of **2, 3**, and **5** from X-ray structural analysis on single crystal (Table 1). The X-ray diffraction data also showed that several crystals from the synthesis of **3** and **5** have similar unit cell parameters. The difference between the value calculated from the expression (100, % - (found content of C, H, N, Cl), %) and the calculated content of metals (Zn, Co, Mn, and Fe) for air-sensitive **1, 4**, and **6** indicates the addition of oxygen to the complex in the course of analysis (about one O_2 molecule per fullerene anion). The addition of O_2 to ionic C_{60} complexes during the elemental analysis was previously reported.[14]

General. UV−visible-NIR spectra were measured in KBr pellets on a Shimadzu-3100 spectrometer in the 240−2600 nm range. FT−IR spectra were measured in KBr pellets with a Perkin-Elmer 1000 series spectrometer (400−7800 cm^{-1}). EPR spectra were recorded from 292 down to 4 K with a JEOL JES-TE 200 X-band ESR spectrometer equipped with a JEOL ES-CT470 cryostat. A Quantum Design MPMS-XL SQUID magnetometer was used to measure static susceptibilities of polycrystalline **1**−**6** between 300 and 1.9 K at 100 mT static magnetic field. A sample holder contribution and core temperature-independent diamagnetic susceptibility (χ_0) were subtracted from the experimental values. The values of Θ and χ_0 were calculated in a high-temperature range using the appropriate formula: $\chi_M = C/(T-\Theta) + \chi_0$.

Crystal Structure Determination. X-ray diffraction data for **2**, **3**, and **5** are listed in Table 2. The intensity data for the structural analysis were collected on a MAC Science DIP-2020K oscillator type X-ray imaging plate diffractometer with graphite monochromated MoK_α radiation at low temperatures using an Oxford Cryostream cooling system. Raw data reduction to F^2 was carried out using the DENZO program.[15] The structures were solved by

(11) (a) Wayland, B. B.; Olson, L. W.; Siddiqui, Z. U. *J. Am. Chem. Soc.* **1970**, *92*, 4235. (b) Kobayashi, H.; Yanagawa, Y. *Bull. Chem. Soc. Jpn.* **1972**, *45*, 450.
(12) Reed, C. A.; Kouba, J. K.; Grimes, C. L.; Cheung, S. K. *Inorg. Chem.* **1978**, *17*, 2666.
(13) Collman, J. P.; Reed, C. A. *J. Am. Chem. Soc.* **1973**, *95*, 2048.
(14) (a) Konarev, D. V.; Khasanov, S. S.; Saito, G.; Otsuka, A.; Yoshida, Y.; Lyubovskaya, R. N. *J. Am. Chem. Soc.* **2003**, *125*, 10074. (b) Allemand, P.-M.; Khemani, K. C.; Koch, A.; Wudl, F.; Holczer, K.; Donovan, S.; Grüner, G.; Thompson, J. D. *Science* **1991**, *253*, 301. (c) Kitagawa, T.; Lee, Y.; Takeuchi, K. *Chem. Commun.* **1999**, 1529.

Table 2. X-ray Diffraction Data for **2**, **3**, and **5**

compound	**2**	**3**	**5**
structural formula	$\{(MDABCO)_2 \cdot CoTPP\} \cdot (C_{60})_2 \cdot (C_6H_4Cl_2)_{4.4} \cdot (C_6H_5CN)_{1.6}$	$\{(MDABCO)_2 \cdot MnTPP\} \cdot (C_{60})_2 \cdot (C_6H_4Cl_2)_{4.2} \cdot (C_6H_5CN)_{1.8}$	$\{(MDABCO)_2 \cdot MnTPP\} \cdot (MDABCO)_2 \{(C_{70})_2\}_2 \cdot (C_6H_4Cl_2)_6 \cdot (C_6H_5CN)_{4.8}$
empirical formula	$C_{215.6}H_{83.6}Cl_{8.8}CoN_{9.6}$	$C_{215.8}H_{83.8}Cl_{8.4}MnN_{9.8}$	$C_{421.6}H_{136}Cl_{12}MnN_{16.8}$
M_r [g·mol^{-1}]	3179.01	3166.25	5916.22
crystal color and shape, size, mm × mm × mm	black, prism 0.5 × 0.4 × 0.3	black, prism 0.4 × 0.3 × 0.2	black, prism 0.6 × 0.5 × 0.16
crystal system	orthorhombic	orthorhombic	triclinic
space group	*Pbca*	*Pbca*	$P\bar{1}$
a, Å	19.8690(10)	20.0250(10)	19.1170(10)
b, Å	26.6500(10)	25.9500(10)	19.5660(10)
c, Å	25.8430(10)	25.938(2)	20.7310(10)
α, °	90	90	67.606(3)
β, °	90	90	81.629(3)
γ, °	90	90	63.610(3)
V, Å^3	13684.1(10)	13478.6(13)	6419.7(6)
Z	4	4	1
ρ_{calc} [g/cm^3]	1.543	1.560	1.530
μ [mm^{-1}]	0.371	0.340	0.256
F(000)	6484	6460	3012
absorption correction	none	none	none
T [K]	180(2)	100(2)	90(2)
max. 2Θ, °	54.56	52.74	54.90
reflns measured	38154	32062	25574
unique reflns	14570	12559	25574
parameters	1105	1105	2721
restraints	347	275	1487
reflns [$F_o > 2\sigma(F_o)$]	10697	8673	19154
R_1 [$F_o > 2\sigma(F_o)$]	0.0583	0.0593	0.0694
wR_2 (all data)[a]	0.1608	0.1479	0.1834
a	0.0725	0.0603	0.0860
b	5.9731	9.5934	7.2534
GOF	1.018	1.008	1.021
restr GOF	1.016	1.001	1.005
CCDC number	610969	610970	610971

[a] $w = 1/[\sigma^2(F_o^2) + (aP)^2 + bP]$, $P = [\mathrm{Max}(F_o^2,0) + 2F_c^2]/3$.

direct method and refined by the full-matrix least-squares method against F^2 using SHELX-97.[16] Non-hydrogen atoms were refined in the anisotropic approximation. Positions of hydrogen atoms were calculated geometrically. Subsequently, the positions of H atoms were refined by the "riding" model with $U_{iso} = 1.2U_{eq}$ of the connected non-hydrogen atom or as ideal CH_3 groups with $U_{iso} = 1.5U_{eq}$.

Molecule Disordering in 2, 3, and 5. (**2** and **3**) $(MDABCO^+)_2 \cdot Co^{II}TPP$ and $(MDABCO^+)_2 \cdot Mn^{II}TPP$ units as well as $C_{60}^{\bullet -}$ radical anions are ordered in **2** and **3**. There are three positions of solvent molecules. One position is occupied by ordered $C_6H_4Cl_2$ molecule. Another one is shared by both C_6H_5CN and $C_6H_4Cl_2$ molecules with 0.9/0.1 occupancies for **2** and 0.8/0.2 occupancies for **3**. The third position is occupied by orientationally disordered $C_6H_4Cl_2$ molecules.

(**5**) $(MDABCO^+)_2 \cdot Mn^{II}TPP$ units and one of crystallographically independent $(C_{70}^-)_2$ dimers are ordered at 100 K. The other $(C_{70}^-)_2$ dimer is fixed in two orientations linked to each other by the rotation about the longer axis of dumb-bell $(C_{70}^-)_2$ at an angle of 36°. The occupancy factors are 0.5/0.5. Noncoordinated $MDABCO^+$ cations are disordered between two orientations linked by their rotation (~10°) about the axis passing through the two nitrogen atoms of $MDABCO^+$. There are six positions of solvent molecules. The two positions are occupied by the ordered C_6H_5CN molecules, whereas in the rest four positions, the solvent molecules are disordered. One of four such positions is partially occupied by the C_6H_5CN molecules, and the other three positions are occupied only by the $C_6H_4Cl_2$ molecules.

Results and Discussion

1. Synthesis. To prepare **1**−**6** we used the reduction of fullerenes with CH_3CH_2SNa in the presence of an excess of MDABCO·I in a $C_6H_4Cl_2/C_6H_5CN$ (19:1) mixture. Then the $(MDABCO^+) \cdot (\text{fullerene}^{\bullet -})$ salt was precipitated from the solution by hexane in the presence of corresponding metalloporphyrins. The data of elemental analysis and compositions of **1**−**6** are listed in Table 1. The compositions of **1, 4**, and **6** determined from elemental analyses and those of **2** and **3** determined from X-ray structural analyses are similar and differ only in the content of solvent $C_6H_4Cl_2$ and C_6H_5CN molecules: $\{(MDABCO)_2 \cdot M^{II}TPP\} \cdot (C_{60(70)})_2 \cdot (C_6H_4Cl_2)_{2.2+x} \cdot (C_6H_5CN)_y$ ($x = 0-2.2$, $y = 0-1.8$). Therefore, all these complexes most probably contain the same $(MDABCO^+)_2 \cdot M^{II}TPP$ units and fullerene anions at a 1:2 molar ratio. **5** has a different composition, $\{(MDABCO)_2 \cdot MnTPP\} \cdot (MDABCO)_2 \cdot \{(C_{70})_2\}_2 \cdot (C_6H_4Cl_2)_6 \cdot (C_6H_5CN)_5$, and involves free noncoordinated $MDABCO^+$ cations additionally to the $(MDABCO^+)_2 \cdot Mn^{II}TPP$ units. We also found that noncoordinating Cu(II) tetraphenylporphyrin does not form such a multicomponent complex, and only $(MDABCO^+) \cdot (C_{60}^-)$ salt can be isolated in the synthesis.

(15) Otwinowski, Z. Minor, W. In *Processing of X-ray diffraction data collection in oscillation mode, Methods in Enzymology*; Carter, C. W., Sweet, R. M., Eds.; Academic Press: 1997; p 276.
(16) Sheldrick, G. M. *SHELX97*; University of Göttingen: Germany, 1997.

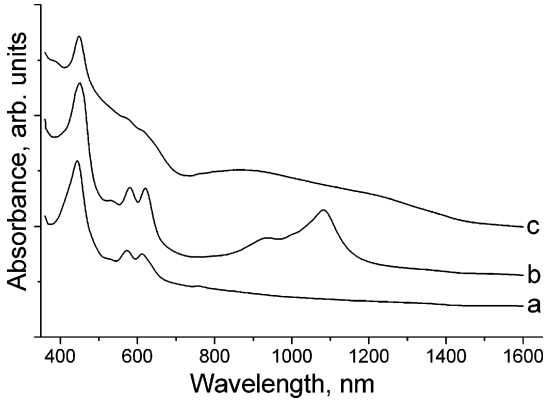

Figure 1. UV−vis-NIR spectra of pristine $Mn^{II}TPP$ (a), **3** (b), and **5** (c) in the 380−1600 nm range.

Table 3. UV−vis-NIR Spectra of Parent Compounds and **1**−**6**

	porphyrin		fullerene	
compd	Soret band, nm	Q-bands, nm	UV-range	NIR-range
C_{60}			262, 341, 470	
C_{70}			-, 420, 540	
ZnTPP	431	553, 596, 623		
CoTPP	421	536, -, 617		
MnTPP	443	-, 572, 611		
FeTPP	427	504, 630, 675		
1	436 (5)	563, 600, -	-, 340	942, 1076
2	425 (4)	532, -, -	-, 340	934, 1077
3	453 (10)	526, 580, 619	-, 340	937, 1083
4	436 (9)	532, 612, -	262, 341	942, 1077
5	449 (6)	-, 574, -	-, -	880, ∼1240
6	434 (7)	-, ∼550, -	-, -	∼860, ∼1240

2. IR− and UV−Visible-NIR Spectra of 1−6. The 1:1 molar ratio between $MDABCO^+$ cations and C_{60} (**1**−**4**) or C_{70} (**5** and **6**) indicates formal −1 charge on the fullerene molecules.

The IR-spectra of **1**−**4** are similar. They manifest the absorption bands of $M^{II}TPP$, $MDABCO^+$, C_{60}, and corresponding solvent molecules (Supporting Information). The position of $F_{1u}(4)$ mode at 1384, 1387, 1395 (split band, **1**), 1382, 1387, 1395 (split band, **2**), 1388 (**3**), and 1387 cm^{-1} (**4**) is close to that in the salts containing −1 charged fullerene.[17] The inversion of the intensities of $F_{1u}(2)$ and $F_{1u}(1)$ modes in the spectra of **1**−**4** is also characteristic of −1 charged C_{60}.[17] The NIR spectra justify the presence of monomeric $C_{60}^{\bullet-}$ in **1**−**4** due to the appearance of characteristic bands at 934−942 and 1076−1083 nm (Figure 1b, Table 3).[18]

The IR spectra of C_{70} complexes **5** and **6** indicate the formation of the $(C_{70}^{-})_2$ dimers, which is proved by the presence of characteristic additional bands (Supporting Information) previously observed even in the complexes and salts containing $(C_{70}^{-})_2$ dimers.[14a,19] NIR spectra justify the formation of $(C_{70}^{-})_2$ dimers as well (two wide characteristic bands at about 880 and 1240 nm) (Figure 1c).[14a,19]

The formation of $(MDABCO^+)_2{\cdot}M^{II}TPP$ units shifts the positions of the Soret bands of metalloporphyrins by 4−10 nm to the red side and in some cases changes the position and relative intensities of the Q-bands at 500−650 nm (Figure 1, Table 3). Similar red shifts of the Soret bands were observed at the coordination of various ligands to metalloporphyrins including fullerenes.[3f,20] It should be noted that the position of the Soret and Q-bands in the spectrum of $Mn^{II}TPP$ obtained by us can even have red shift relative to pristine metalloporphyrin due to the coordination of ethanol,[12] which was used as a solvent in the syntheses.

3. Crystal Structures of $\{(MDABCO)_2{\cdot}Co^{II}TPP\}{\cdot}(C_{60})_2{\cdot}(C_6H_4Cl_2)_{4.4}{\cdot}(C_6H_5CN)_{1.6}$ (2) and $\{(MDABCO)_2{\cdot}Mn^{II}TPP\}{\cdot}(C_{60})_2{\cdot}(C_6H_4Cl_2)_{4.2}{\cdot}(C_6H_5CN)_{1.8}$ (3). Complexes **2** and **3** are isostructural. Metalloporphyrins coordinate two $MDABCO^+$ cations in both **2** and **3**. Therefore, metal atoms are six-coordinated and have an octahedral environment at M^{II} centers (M = Co and Mn, Figure 2a). Previously such an environment was reported for $Co^{II}TPP$ in $(piperidine)_2{\cdot}Co^{II}TPP$[21] and by our knowledge was for the first time found for $Mn^{II}TPP$ since even in a large excess of N-containing ligands such as pyridine and imidazole (L) $Mn^{II}TPP$ forms only five-coordinated $L{\cdot}Mn^{II}TPP$.[12] Most probably, crystal packing forces in the complex with fullerene facilitate the stabilization of these six-coordinated metalloporphyrins. The Co− and Mn−N($MDABCO^+$) distances of 2.475(2) and 2.553(2) Å indicate weak coordination of $MDABCO^+$ cations to metalloporphyrins. The Co−N($MDABCO^+$) distances are essentially shorter in six-coordinated $(MDABCO^+){\cdot}Co^{II}OEP{\cdot}(C_{60}^{-})$ units (in these units C_{60}^{-} additionally coordinates to $Co^{II}OEP$ with the Co−C(C_{60}^{-}) distance of 2.508(4) Å at 100 K)[8] and five-coordinated $(MDABCO^+){\cdot}Co^{II}TMPP$ (2.340(3) and 2.385(2) Å, respectively).[8,10] The elongation of Co−N axial coordination bonds from 2.157-(3) to 2.436(2) Å was observed at the transition from five-coordinated (imidazole)·$Co^{II}TPP$ to six-coordinated $(piperidine)_2{\cdot}Co^{II}TPP$. This elongation is a consequence of that an unpaired electron involved in the bonding is located in the d_{z^2} orbital, which pointed directly to the two nitrogen atoms of axial ligands.[21] The removal of the electron from d_{z^2} orbital in $Co^{III}TPP^+$ leads to a noticeable shortening of axial Co−N bonds in $(piperidine)_2{\cdot}Co^{III}TPP^+$ to 2.060(3) Å.[22] For the same reason, the Mn−N axial coordination bonds can be elongated and the $(MDABCO)_2{\cdot}Mn^{II}TPP$ units can be destabilized. This implies that an unpaired electron of $Mn^{II}TPP$ involved in the bonding with $MDABCO^+$ should also localize on d_{z^2} orbital. Additional contribution to the elongation of M−N bonds in the $(MDABCO^+)_2{\cdot}M^{II}TPP$ (M = Co and Mn) can provide the repulsion between two positive charges of the $MDABCO^+$ cations. Porphyrin macrocycles are nearly planar with root-mean-square devia-

(17) (a) Picher, T.; Winkler, R.; Kuzmany, H. *Phys. Rev. B* **1994**, *49*, 15879. (b) Semkin, V. N.; Spitsina, N. G.; Krol, S.; Graja, A. *Chem. Phys. Lett.* **1996**, *256*, 616.
(18) Reed, C. A.; Bolskar, R. D. *Chem. Rev.* **2000**, *100*, 1075.
(19) Konarev, D. V.; Khasanov, S. S.; Vorontsov, I. I.; Saito, G.; Antipin, Yu. A.; Otsuka, A.; Lyubovskaya, R. N. *Chem. Commun*. **2002**, 2548.
(20) (a) Wayland, B. B.; Minkiewicz, J. V.; Abd-Elmageed, M. E. *J. Am. Chem. Soc.* **1974**, *96*, 2795. (b) Litvinov, A. L.; Konarev, D. V.; Kovalevsky, A. Yu.; Coppens, P.; Lyubovskaya, R. N. *Cryst. Growth Des.* **2005**, *5*, 1807.
(21) (a) Scheidt, W. R. *J. Am. Chem. Soc.* **1974**, *96*, 90. (b) Scheidt, W. R. *J. Am. Chem. Soc.* **1974**, *96*, 84.
(22) Scheidt, W. R.; Cunningham, J. A.; Hoard, J. L. *J. Am. Chem. Soc.* **1973**, *95*, 8289.

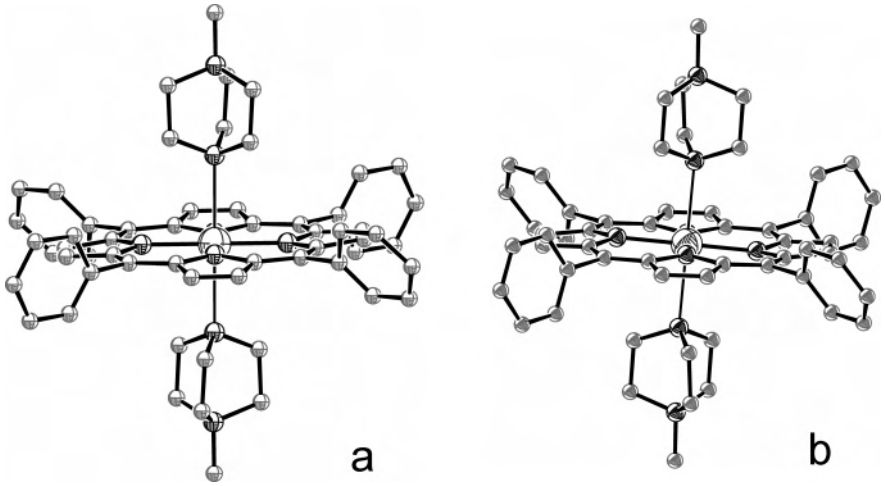

Figure 2. Molecular structure of $(MDABCO^+)_2 \cdot Mn^{II}TPP$ units in **3** (a) and **5** (b). $(MDABCO^+)_2 \cdot Co^{II}TPP$ units in **2** have geometry similar to that of $(MDABCO^+)_2 \cdot Mn^{II}TPP$ in **3**.

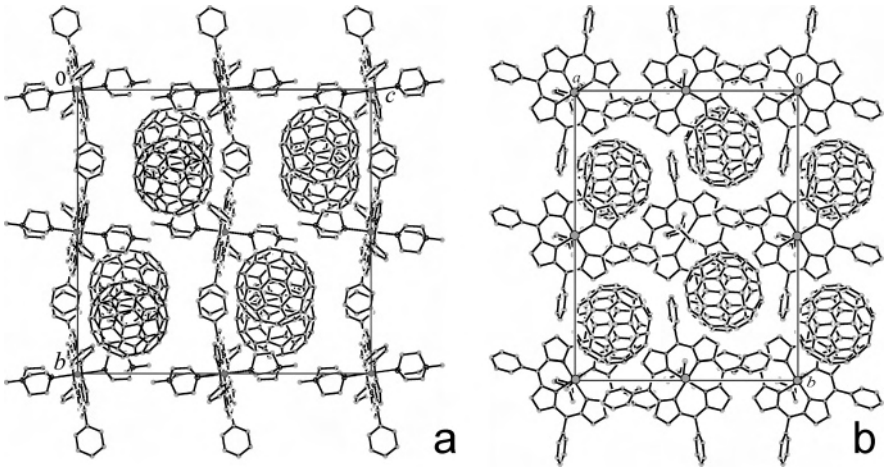

Figure 3. View of the crystal structure of **2** along the *a* (a) and *c* axes (b). Solvent $C_6H_4Cl_2$ and C_6H_5CN molecules are omitted for clarity. Only one of two coordinating $MDABCO^+$ cations is shown in part (b).

tions rms = 0.033 and 0.064 Å for **2** and **3**. Co atom is in the porphyrin plane with the average length of the equatorial Co−N bonds of 1.988(2) Å), which is close to that observed for six-coordinated $(piperidine)_2 \cdot Co^{II}TPP$ (1.987(2) Å).[21] A thermal parameter of Mn^{II} atom for the vibration perpendicular to the mean plane of the core was higher than that of the N atom (rms amplitudes are 0.055 Å and 0.047 Å, respectively). The disorder model in which a metal atom was distributed between two symmetry equivalent out-of-plane positions with isotropic temperature factors gives the displacement parameter of ±0.127 Å. However, the accuracy of the crystal structure determination for **3** does not allow one to refine simultaneously the position of Mn^{II} atoms with anisotropic temperature factors because they show large correlations. Similarly for high-spin ($S = 5/2$) $Mn^{II}TPP \cdot (C_6H_5CH_3)_2$ the out-of-plane displacement of Mn^{II} atom was calculated to be ~0.177 Å. The length of equatorial Mn−N bonds is average in **3** at 2.096(2) Å and is close to that in $Mn^{II}TPP \cdot (C_6H_5CH_3)_2$ (2.084(2) Å).[23]

(23) Kirner, J. F.; Reed, C. A.; Scheidt, W. R. *J. Am. Chem. Soc.* **1977**, *99*, 1093.

The $(MDABCO)_2 \cdot M^{II}TPP$ units form channels passing along the *a*-axis (Figure 3a shows the view along four such channels) and accommodate zigzag chains of the $C_{60}^{\bullet -}$ with relatively short interfullerene center-to-center distances of 10.342 and 10.428 Å for **2** and **3**, respectively (Figure 3b). There are interfullerene C−C contacts of 3.558−3.729 Å in **2** and noticeably longer ones in **3** (3.716−3.918 Å). The center-to-center distances between $C_{60}^{\bullet -}$ in two other directions are about or more than 13.5 Å. Each $C_{60}^{\bullet -}$ is surrounded by three $MDABCO^+$ cations with multiple short van der Waals C−C and H−C contacts of 3.529−3.842 and 2.647−2.862 Å length. The π-interaction and coordination of $C_{60}^{\bullet -}$ to $M^{II}TPP$ are absent (the shortest Co and Mn···C($C_{60}^{\bullet -}$) distances are 6.26 and 6.31 Å). Several short van der Waals C···C contacts are only formed between phenyl substituents of metalloporphyrins and fullerenes. Metalloporphyrins are isolated from one another (the shortest M^{II}···M^{II} distances are 16.3 and 16.4 Å for **2** and **3**). Due to the large size of the channels formed by porphyrins there is a large space in them occupied by disordered solvent $C_6H_4Cl_2$ and C_6H_5CN molecules.

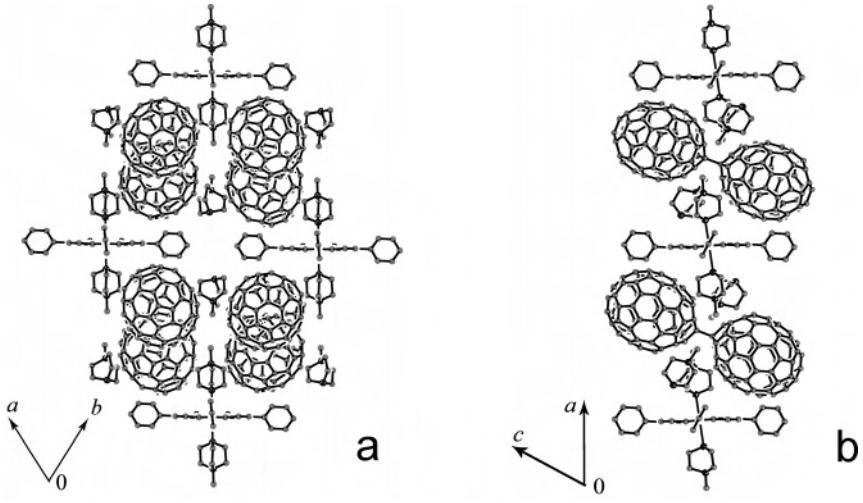

Figure 4. View of the crystal structure of **5** approximately along the *c*-axis (a) and in the *ac*-plane (b). $C_6H_4Cl_2$ and C_6H_5CN molecules are omitted for clarity.

Table 4. SQUID Data for the Complexes **1** and **3**−**6** in the 1.9−300 K Range

compd	Θ, K (temp range, K)	observed magnetic moment, μ_B	calculated magnetic moment, μ_B
1	−13 (100−300)	1.6 (100−300)[a]	1.73 (S = 1/2 ($C_{60}^{\bullet-}$), 0 (ZnTPP)[a]
3	−2 (70−300)	4.1 (70−300)[a]	4.53 (S = 1/2 ($C_{60}^{\bullet-}$), 5/2 (Mn^{II}TPP))[a]
4	−2 (70−300)	3.7 (70−300)[a]	3.87 (S = 1/2 ($C_{60}^{\bullet-}$), 2 (Fe^{II}TPP))[a]
5	0 (10−300)	5.3 (10−300)[b]	5.92 (S = 5/2 (Mn^{II}TPP))[b]
6	−31 (150−300)	4.3 (150−300)[b]	4.90 (S = 2 (Fe^{II}TPP)[b]

[a] Magnetic moment was calculated per half of formula unit $\{(MDABCO)_2 \cdot M^{II}TPP\}_{0.5} \cdot C_{60} \cdot (C_6H_4Cl_2)_x \cdot (C_6H_5CN)_y$ containing one $C_{60}^{\bullet-}$ and half of M^{II}TPP. [b] Magnetic moment was calculated per formula unit containing one $(C_{70}^{-})_2$ dimer and one M^{II}TPP.

$\{(MDABCO)_2 \cdot Mn^{II}TPP\} \cdot (MDABCO)_2 \cdot \{(C_{70})_2\}_2 \cdot (C_6H_4Cl_2)_3 \cdot (C_6H_5CN)_2$ (5). Two $MDABCO^+$ cations coordinate to Mn^{II}TPP in **5** (Figure 2b). The geometric parameters of $(MDABCO)_2 \cdot Mn^{II}$TPP units are nearly the same as those in **3**. Coordinated nitrogen atoms of two $MDABCO^+$ cations and a metal atom lie along a straight line in **2, 3**, and **5**, which is nearly perpendicular to the porphyrin plane in **2** and **3** (88°) and forms an angle of 85° in **5**. In previously described $(piperidine)_2 \cdot Co^{II}$TPP this line forms an angle of about 89° with the porphyrin plane.[21a] The porphyrin macrocycle is unusually deformed in **5** in such a way that the nitrogen atoms of two pyrrole rings come out by 0.120 Å above and below the porphyrin plane. The Mn−N($MDABCO^+$) distance in **5** is 2.511(3) Å. Thermal parameters of Mn^{II} atom were almost the same as for N atoms of the porphyrin macrocycle, and there was no reason to consider the disordered model with the out-of-plane displacement of Mn^{II}. The average lengths of Mn−N equatorial bonds of 2.097(2) Å are close to those in **3** and high-spin (S = 5/2) $Mn^{II}TPP \cdot (C_6H_5CH_3)_2$.[23]

In accordance with optical data, the $C_{70}^{\bullet-}$ radical anions form single-bonded $(C_{70}^{-})_2$ dimers in **5** (Figure 4a,b). The length of the intercage C−C bond in the ordered dimer of 1.601(4) Å is close to that in previously described single-bonded $(C_{70}^{-})_2$ dimers (1.584(9) Å).[19] The $(C_{70}^{-})_2$ dimers form closely packed layers arranged almost parallel to the *c*-axis. Each C_{70}^{-} anion in the layer forms short van der Waals C−C contacts with three other C_{70}^{-} anions from neighboring dimers (the shortest C−C contacts are in the 3.162−3.341 Å range). Each $(C_{70}^{-})_2$ dimer is surrounded by four $MDABCO^+$ cations located close to the interfullerene C−C σ-bond. Since electrons on the LUMO of C_{70}^{-} should participate in the formation of the interfullerene σ-bond of the $(C_{70}^{-})_2$ dimer, two negative charges can localize near this bond, and such an arrangement of $MDABCO^+$ cations provides better conditions for the electrostatic interaction between positive and negative charges in **5**. The layers from $(C_{70}^{-})_2$ dimers alternate with the layers composed of $(MDABCO^+)_2 \cdot Mn^{II}$TPP units and noncoordinating $MDABCO^+$ cations (Figure 4a). Mn^{II}TPP are completely isolated from one another with the closest Mn...Mn distance larger than 19 Å. Most parts of solvent molecules are located in large cavities formed by phenyl substituents of Mn^{II}TPP and $(C_{70}^{-})_2$ dimers (Figure 4a). Due to the large size of this cavity solvent molecules are strongly disordered.

4. Magnetic Properties of the Complexes. a. $\{(MDABCO^+)_2 \cdot Zn^{II}TPP\} \cdot (C_{60}^{\bullet-})_2 \cdot (C_6H_4Cl_2)_{2.5} \cdot (C_6H_5CN)_{0.5}$ (1). Zn^{II}TPP is diamagnetic (S = 0) and EPR silent that allows one to study magnetic interaction between $C_{60}^{\bullet-}$ except for a contribution from metalloporphyrin. Magnetic moment of **1** (1.6 μ_B) at 300 K is close to 1.73 μ_B calculated for a system of noninteracting 1/2 spins per $\{(MDABCO^+)_2 \cdot Zn^{II}TPP\}_{0.5} \cdot (C_{60}^{\bullet-})$ unit (Table 4). Magnetic moment is temperature independent down to 100 K, and below this temperature it decreases down to 0.5 μ_B at 1.9 K (Figure 5a). Magnetic susceptibility of **1** follows the Curie−Weiss law in the 300−100 K range with a negative Weiss constant of −13 K and manifests a maximum at 10 K. The EPR signal of **1** at 293 K is a single Lorentzian line with g = 2.0000 and the line width of 2.75 mT. The g-factor of the signal remains unchanged down to 120−100 K, and the signal strongly narrows with the temperature decrease (Figure

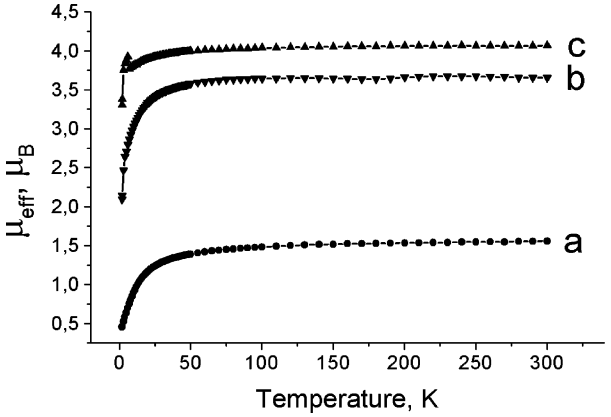

Figure 5. Temperature dependences of magnetic moments of polycrystalline **1** (a), **4** (b), and **3** (c) in the 1.9−300 K range.

6a,b), which is characteristic of $C_{60}^{\bullet-}$.[18] Below 120−100 K the signal splits into two components shifted to higher and lower magnetic fields with the temperature decrease and slightly broadens ($g_1 = 1.9986$, $\Delta H = 0.35$ mT and $g_2 = 2.0007$, $\Delta H = 0.19$) (Figure 6a,b). Integral intensity of the signal at 293 K corresponds to the contribution of one 1/2 spin per $\{(MDABCO^+)_2 \cdot Zn^{II}TPP\}_{0.5} \cdot (C_{60}^{\bullet-})$ unit. The dependence of (integral intensity of the signal $\times$ T) vs T is linear, and the $I \times T$ value decreases below 100 K (in accordance with SQUID data). At 4 K less than 10% of $C_{60}^{\bullet}$ spins contribute to spin susceptibility of **1**. Such magnetic behavior indicates the antiferromagnetic interaction between $C_{60}^{\bullet-}$ spins in **1**, which manifests itself already below 120−100 K. It can be supposed that the observed antiferromagnetic interaction of $C_{60}^{\bullet-}$ spins is realized in **1** in the chains similar to those observed in **2** and **3**. In this case we can estimate the exchange interaction according to the one-dimensional Heisenberg antiferromagnetic model with $J/k_B = -9.6$ K (Supporting Information).

b. $\{(MDABCO^+)_2 \cdot Fe^{II}TPP\} \cdot (C_{60}^{\bullet-})_2 \cdot (C_6H_4Cl_2)_{2.2} \cdot (C_6H_5CN)_{0.8}$ (4). Magnetic moment of **4** is 3.7 μ_B per $\{(MDABCO^+)_2 \cdot Fe^{II}TPP\}_{0.5} \cdot (C_{60}^{\bullet-})$ unit at 300 K (Table 4, Figure 5b). The value calculated for the system containing monomeric $C_{60}^{\bullet-}$ ($S = 1/2$) and $Fe^{II}TPP$ in high spin state ($S = 2$) is 3.87 μ_B. The spin state of $L_2 \cdot Fe^{II}TPP$ is known to depend on the ligand strength of "L". $Fe^{II}TPP$ coordinating two strong field ligands such as pyridine, imidazole, or piperazine is diamagnetic ($S = 0$), whereas $Fe^{II}TPP$ coordinating two weak field tetrahydrofuran ligands has a high spin state ($S = 2$) with a magnetic moment of 5.1 μ_B.[13,24] Therefore, the retention of the high spin state of $Fe^{II}TPP$ at the coordination of two $MDABCO^+$ is possible if they are weak-field ligands. The positive charge in $MDABCO^+$ cations can essentially weaken their ligand strength in comparison with neutral bidentant DABCO. Indeed, the Co···N($MDABCO^+$) distance in the $(MDABCO^+) \cdot Co^{II}TMPP$ of 2.385(2) Å[10] is noticeably longer than the distance of 2.157(3) Å in (imidazole)·$Co^{II}TPP$.[21b] Similarly, the Fe···O distance of 2.351(3) Å with a weak-field THF ligand in $(THF)_2 \cdot Fe^{II}TPP$[24a] is noticeably longer than the Fe···N distance of 2.014(5) Å in $(imidazole)_2 \cdot Fe^{II}TPP$.[24b] The Weiss constant of −2 K (70−300 K) indicates weak antiferromagnetic interaction of spins in **4**, and the magnetic moment of **4** begins to decrease below 70 K (Figure 5b). $Fe^{II}TPP$ shows no EPR signal. The parameters of the EPR signal of **4** are close to those observed for $C_{60}^{\bullet-}$ ($g = 1.9949$ and $\Delta H = 16.4$ mT at 293 K). The g-factor value is nearly temperature independent down to 120 K, and the signal noticeably narrows with the temperature decrease. Below 120−100 K the EPR signal of **4** splits into two components, which shift to higher and lower magnetic fields with the temperature decrease and noticeably broaden ($g_1 = 1.9708$, $\Delta H = 8$ mT; $g_2 = 2.0001$, $\Delta H = 17.6$ mT) (Figure 7a,b). Such behavior is similar to that of **1** and can be attributed to the antiferromagnetic interaction of $C_{60}^{\bullet-}$ spins. It is interesting to note that in spite of the fact that $Fe^{II}TPP$ is EPR silent (as $Zn^{II}TPP$ in **1**), the parameters of the EPR signal in **4** (g-factor and line width) are noticeably different relative to those of the EPR signal in **1** (Figures 6 and 7).

c. $\{(MDABCO^+)_2 \cdot Co^{II}TPP\} \cdot (C_{60}^{\bullet-})_2 \cdot (C_6H_4Cl_2)_{4.4} \cdot (C_6H_5CN)_{1.6}$ (2). The magnetic properties of **2** were studied by temperature-dependent EPR on a single-crystal sample tested by X-ray diffraction. The EPR signal in **2** has a Lorentzian shape, which does not depend on the orientation of the crystal in the 4−293 K range. The signal has $g = 2.1082$ and a line halfwidth of 7.1 mT at 293 K (Figure 8a,b). The observed g-factor value is an intermediate one between those characteristic of $C_{60}^{\bullet-}$ (1.9996−2.0000)[18] and six-coordinated $(piperidine)_2 \cdot Co^{II}TMPP$ (an asymmetric signal with $g_\perp = 2.214$ and $g_{II} = 2.054$).[25] Therefore, that can be a signal appeared due to the exchange coupling between $C_{60}^{\bullet-}$ and $(MDABCO^+)_2 \cdot Co^{II}TPP$. The exchange interaction averages g-factor value and results in the disappearance of individual features of the signals (asymmetry, hyperfine splitting, and etc). A similar single line ($g = 2.1188$ and $\Delta H = 52$ mT at 292 K) was observed in $\{(MDABCO^+) \cdot Co^{II}OEP \cdot (C_{60}^{-})\} \cdot (C_6H_4Cl_2)_{1-x} \cdot (C_6H_5CN)_x$ ($x \cong 0.67$) with nonbonded $Co^{II}OEP$ and $C_{60}^{\bullet-}$ species above 50 K.[8] One Co^{II}-OEP and one $C_{60}^{\bullet-}$ contribute to the EPR signal in the $Co^{II}OEP$ complex, whereas one $Co^{II}TPP$ and two $C_{60}^{\bullet-}$ contribute to the EPR signal in **2**. As a result, the signal in **2** shifts closer to g-factors characteristic of $C_{60}^{\bullet-}$ and becomes essentially narrower (7.1 vs 52 mT). Similar single lines instead of two signals were observed in other ionic complexes and salts of C_{60} containing paramagnetic cations and $C_{60}^{\bullet-}$.[6a,b,d,14a] The temperature decrease narrows the signal ($\Delta H = 3.55$ mT at 85 K). Below 70 K the g-factor shifts to larger values with the temperature decrease and broadens ($g = 2.1907$, $\Delta H = 5.2$ mT at 4 K, Figure 8a,b). The temperature dependence of integral intensity of the signal multiplied by T ($I \times T$) is linear, and the $I \times T$ value decreases below 35 K showing antiferromagnetic interaction of spins at low temperatures (Supporting Information). According to X-ray diffraction data **2** contains closely packed

(24) (a) Jameson, G. B.; Molinaro, F. S.; Ibers, J. A.; Collman, J. P.; Brauman, J. I.; Rose, E. J.; Suslick, K. S. *J. Am. Chem. Soc.* **1980**, *102*, 3224. (b) Reed, C. A.; Mashiko, T.; Scheidt, W. R.; Spartalian, K.; Lang, G. *J. Am. Chem. Soc.* **1980**, *102*, 2302.

(25) Walker, A. F. *J. Am. Chem. Soc.* **1970**, *92*, 4235.

(26) Paul, P.; Kim, K.-C.; Sun, D.; Boyd, P. D. W.; Reed, C. A. *J. Am. Chem. Soc.* **2002**, *124*, 4394.

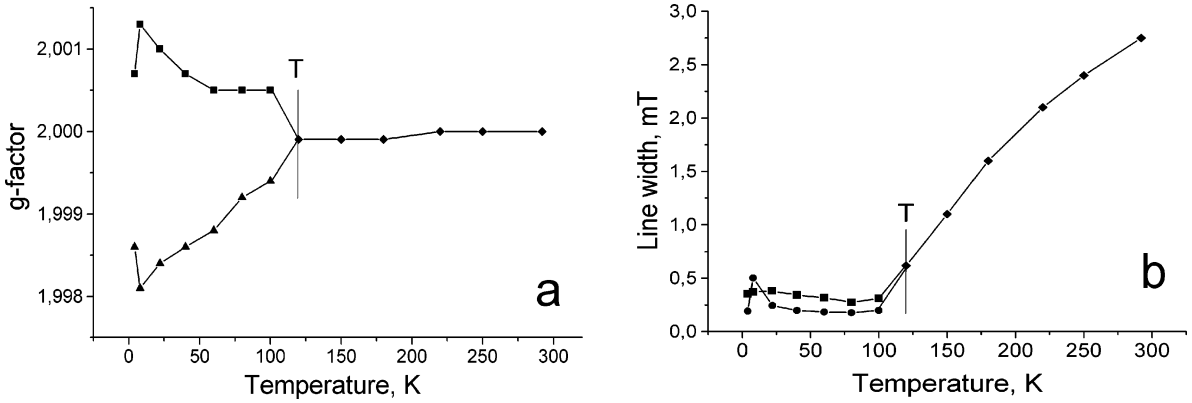

Figure 6. Temperature dependence of parameters of the EPR signal in **1** attributed to $C_{60}^{\bullet-}$ in the 4−293 K range: *g*-factor (a) and line width (b).

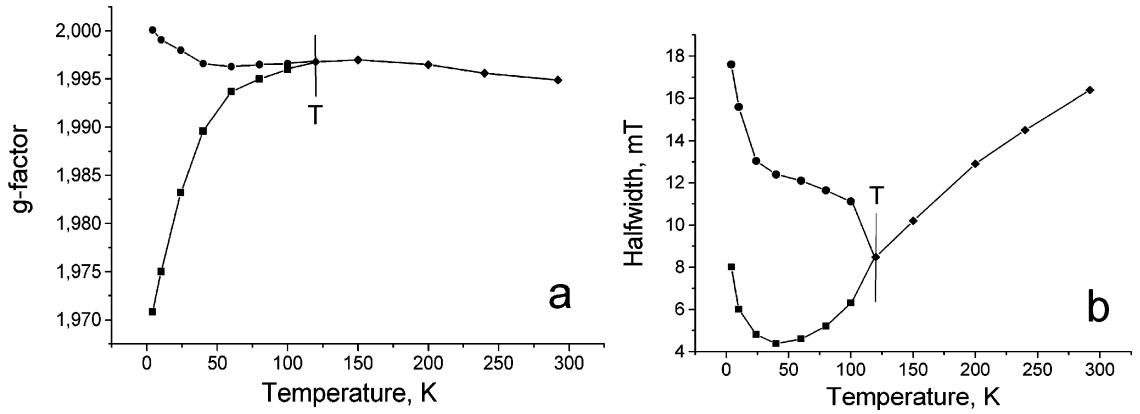

Figure 7. Temperature dependence of EPR parameters of the signal in **4** attributed to $C_{60}^{\bullet-}$ in the 4−293 K range: *g*-factor (a) and line width (b).

zigzag chains of $C_{60}^{\bullet-}$, and antiferromagnetic interactions can realize namely in this chains decreasing the contribution of $C_{60}^{\bullet-}$ spins to the EPR signal. As a result, the *g*-factor of EPR signal in **2** shifts closer to that characteristic of individual six-coordinated $Co^{II}TPP$.

d. $\{(MDABCO^{+})_2 \cdot Mn^{II}TPP\} \cdot (C_{60}^{\bullet-})_2 \cdot (C_6H_4Cl_2)_{4.2} \cdot (C_6H_5CN)_{1.8}$ **(3).** Magnetic moment of **3** is equal to 4.1 μ_B per $\{(MDABCO^{+})_2 \cdot Mn^{II}TPP\}_{0.5} \cdot (C_{60}^{\bullet-})$ unit at 300 K and begins to decrease below 70 K (Figure 5c). The value calculated for the system containing noninteracting $C_{60}^{\bullet-}$ ($S = 1/2$) and high spin $Mn^{II}TPP$ ($S = 5/2$) is 4.53 μ_B. The geometric parameters of the $Mn^{II}TPP$ porphyrin in **3** are also evidence of the high spin state of $Mn^{II}TPP$.[23] The Weiss constant of **3** is negative (−2 K) in the 70−300 K range. The EPR signal of **3** is very broad (more than 100 mT) and cannot be fitted well by one Lorentzian line (Figure 9). The approximate *g*-factor value of 2.4 can be considered as an intermediate one between those of $C_{60}^{\bullet-}$ (1.9996−2.0000) and high spin $Mn^{II}TPP$ ($g_{\perp} = 5.96$ and $g_{||} = 2.00$[12]). Therefore, this signal can appear due to exchange coupling between $C_{60}^{\bullet-}$ and $(MDABCO^{+})_2 \cdot Mn^{II}TPP$ similarly to **2**. The shape of the signal is not changed down to 100 K, below which it becomes closer to an asymmetric signal characteristic of high spin $Mn^{II}TPP$.[12] *g*-factor also shifts to larger values ($g = 4.9$ at 4 K). High spin $Mn^{II}TPP$ has $g = 5.96$.[12] Such magnetic behavior most probably can be explained by the antiferromagnetic interaction of spins in the $C_{60}^{\bullet-}$ chains. The distance between $C_{60}^{\bullet-}$ of 10.428 Å in the chains is rather long (longer than that distance in **2** and 10.18 Å van der Waals diameter of C_{60}) that results in weak magnetic interaction in **3**.

e. $\{(MDABCO^{+})_2 \cdot Mn^{II}TPP\} \cdot (MDABCO^{+})_2 \cdot \{(C_{70}^{-})_2\}_2 \cdot (C_6H_4Cl_2)_6 \cdot (C_6H_5CN)_5$ **(5).** According to the X-ray diffraction and optical data **5** contains diamagnetic single bonded $(C_{70}^{-})_2$ dimers.[14a] That results in drastic changes in the magnetic behavior of **5** relative to **1**−**4**. The magnetic moment of **5** is equal to 5.3 μ_B, whereas the calculated magnetic moment for the high spin $Mn^{II}TPP$ is 5.92 μ_B. Structural parameters for the $(MDABCO^{+})_2 \cdot Mn^{II}TPP$ units in **5** also justify the high spin state of $Mn^{II}TPP$. The magnetic moment is temperature independent down to 10 K (Supporting Information), and the Weiss constant is close to zero. Therefore, the disappearance of the contribution of $C_{70}^{\bullet-}$ spins destroys magnetic exchange interactions of spins in **5.** Paramagnetic $(MDABCO^{+})_2 \cdot Mn^{II}TPP$ units are completely magnetically isolated due to large distances between Mn^{II} centers. In the EPR spectrum of **5** we found low-field six-line pattern with an average $g = 5.96$ and line splitting with $B = 65.8 \times 10^{-4}$ cm^{-1} (7 mT) due to a hyperfine interaction (HFI) with ^{55}Mn nuclei ($I = 5/2$). The signal at *g*-factor 2.000 with unresolved splitting was also observed (Figure 10). These signals can be attributed to the $g_{\perp}$ and $g_{||}$ components of the spectrum[12] and justify the high spin state of Mn^{II} in six-coordinated $(MDABCO^{+})_2 \cdot Mn^{II}TPP$ units. Additionally to the major signal, split and weak signals are also observed in the magnetic field from 130 up to 300 mT (Figure 10). The

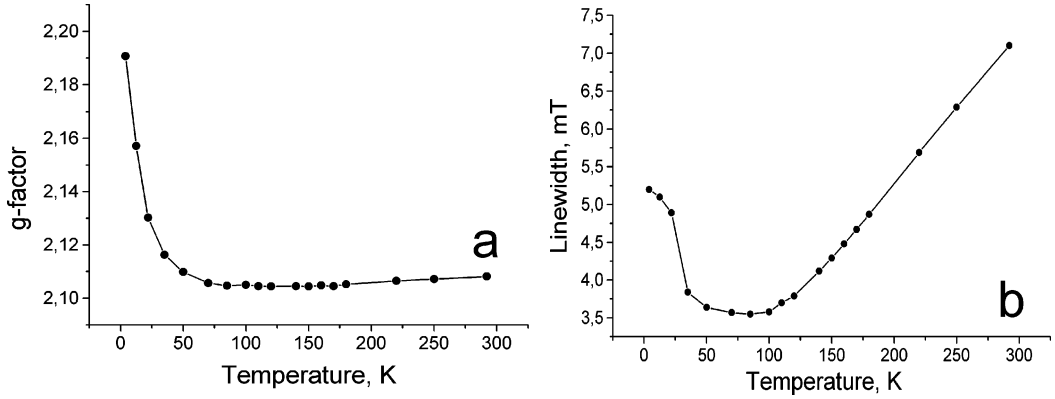

Figure 8. Temperature dependence of EPR parameters of the signal in **2** in the 4−293 K range: *g*-factor (a) and line width (b).

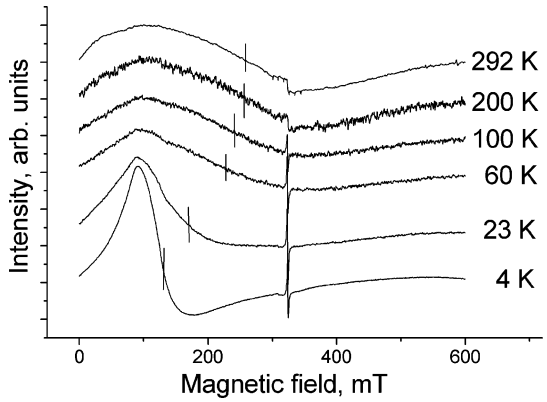

Figure 9. Temperature dependence of the shape of EPR signal observed in **3** from 293 down to 4 K. Weak narrow signal at about 323 mT is associated with impurities (most probably due to the reduction of $C_{120}O$ impurity).[26]

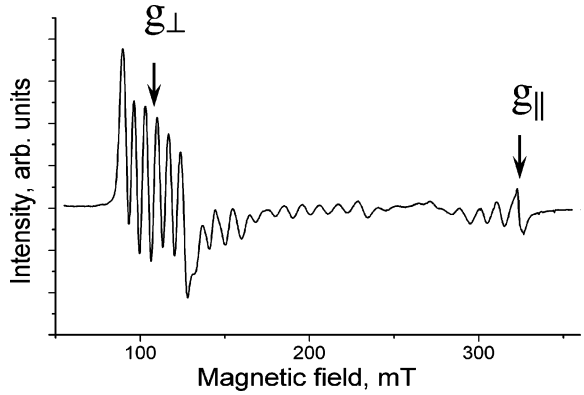

Figure 10. EPR signal of **5** at 293 K attributed to six-coordinated $(MDABCO^+)_2{\cdot}Mn^{II}TPP$ units.

average splitting is about 10 mT that can be associated with HFI with ^{55}Mn nuclei. However, because of the overlapping it is impossible to determine exactly the positions of these additional signals. These signals can manifest due to a slight distortion of Mn^{II} centers in $(MDABCO^+)_2{\cdot}Mn^{II}TPP$ from a regular octahedral environment[27] or due to the polycrystallinity of the sample.

The composition of $\{(MDABCO^+)_2{\cdot}Fe^{II}TPP\}{\cdot}(C_{70}^-)_2{\cdot}(C_6H_4Cl_2)_3$ (**6**) is similar to those of **1**−**4.** According to optical data it contains diamagnetic single bonded $(C_{70}^-)_2$ dimers. Unfortunately, the crystal structure of **6** is unknown, and that prevents us from analyzing the magnetic properties of this complex in detail. The magnetic moment of **6** is equal to 4.3 μ_B. The complex is EPR silent in the 4−293 K range that is consistent with the presence of EPR silent $(C_{70}^-)_2$ dimers and $Fe^{II}TPP$. Though **6** contains diamagnetic $(C_{70}^-)_2$ dimers, the Weiss constant of −31 K is relatively large in the 150−300 K range, and the magnetic moment in **6** decreases below 120 K (Supporting Information).

Conclusions

A new series of ionic complexes comprising C_{60} and C_{70} anions and coordinating $(MDABCO^+)_2{\cdot}M^{II}TPP$ assemblies (M = Zn, Co, Mn, Fe) were obtained. The use of coordination cations such as $MDABCO^+$ [this work and refs 8 and 10] demonstrates a high synthetic potential for the design of a variety of ionic fullerene compounds with five- and six-coordinated metalloporphyrins with various substituents and metals (Zn^{II}, Co^{II}, Mn^{II}, and Fe^{II}). This allows one to obtain new coordination assemblies with $MDABCO^+$ or other coordination cations, unknown so far, which can have new structures and properties. For example, complex formation with fullerene anions stabilizes six-coordinated $Mn^{II}TPP$ porphyrins in the solid state, which were not found previously most probably due to their low stability. Indeed, the M−N bonds are very weak in both coordination $(MDABCO^+)_2{\cdot}M^{II}TPP$ assemblies with the length of 2.475(2) Å for M = Co and 2.511(3)−2.553(2) Å for M = Mn.

Complexes contain $(MDABCO^+)_2{\cdot}M^{II}TPP$ units with a different spin state. $Zn^{II}TPP$ is diamagnetic ($S = 0$), $Co^{II}TPP$ presumably has $S = 1/2$ spin state, whereas $Mn^{II}TPP$ and $Fe^{II}TPP$ are most probably in a high spin state. Complexes **1**−**4** are interesting examples of compounds, in which fullerene anions are neither dimerized nor coordinated but are located close enough to each other to realize magnetic exchange interaction between them. This interaction is obviously an antiferromagnetic one and decreases the magnetic moments of the complexes below 120−70 K. The presence of paramagnetic $(MDABCO^+)_2{\cdot}M^{II}TPP$ (M = Co, Mn, and Fe (**2**−**4**)) units does not affect noticeably the temperatures (70−100 K) at which the decrease of magnetic moments is observed relative to **1** containing diamagnetic $Zn^{II}TPP$ (120−100 K). The negative Weiss constant is also the highest for **1** among **1**−**4**. That can be explained by the

(27) Goodgame, D. M. L.; El Mkami, H.; Smith, G. M.; Zhao, J. P.; McInnes, E. J. L. *Dalton Trans.* **2003**, 34.

absence of strong direct magnetic exchange interaction between M^{II} centers and $C_{60}^{\bullet-}$ due to large distances between them. However, some modifications of EPR spectra of **1**−**4** are observed due to the different spin states of metalloporphyrins. Only $C_{60}^{\bullet-}$ spins manifest itself in **1** and **4** containing EPR silent Zn^{II}TPP and Fe^{II}TPP. In this case antiferromagnetic interaction of spins split single EPR signals into two components below 120−80 K, which broaden and shift to lower and higher magnetic fields with the temperature decrease. In **2** and **3** Co^{II}TPP and Mn^{II}TPP are EPR active. These complexes manifest single EPR signals with *g*-factors intermediate between those characteristic of $C_{60}^{\bullet-}$ and corresponding metalloporphyrins as a result of exchange coupling between these paramagnetic species. Single EPR lines instead of two lines were previously observed for different ionic complexes and salts of C_{60} containing two EPR active species: cations and $C_{60}^{\bullet-}$.[6a,b,d,14a] Most probably this interaction is weak and realized only through the diamagnetic phenyl substituents and $MDABCO^{+}$ cations. In both cases antiferromagnetic ordering of $C_{60}^{\bullet-}$ spins at low temperatures (<80 K) lowers the number of unpaired $C_{60}^{\bullet-}$ spins relative to the number of spins of metalloporphyrins and shifts *g*-factors of **2** and **3** closer to those characteristic of individual metalloporphyrins. A similar magnetic behavior was found in ionic multicomponent complexes of tetrabenzyl-*p*-phenylenediamine with fullerene: $(TBPDA)_2{\cdot}(C_{60}^{\bullet-}){\cdot}(D^{+}_{1-3})$ containing cations D^{+}_{1-3} with a different spin state (D_1 = decamethylcobaltocene, $Cp^*_2Co^{+}$ has $S = 0$; D_2 = $TDAE^{\bullet+}$ has $S = 1/2$; and D_3 = decamethylchromocene, $Cp^*_2Cr^{+}$ has $S = 3/2$).[28] These complexes show the weak antiferromagnetic interaction of $C_{60}^{\bullet-}$ spins most probably mediated by phenylene groups of TBPDA. The substitution of diamagnetic $Cp^*_2Co^{+}$ by paramagnetic $TDAE^{\bullet+}$ and $Cp^*_2Cr^{+}$ does not affect noticeably the temperature at which the magnetic moment of the complexes decreases. However, the complexes demonstrate single EPR signals due to the exchange coupling between $C_{60}^{\bullet-}$ and corresponding cations.[28] Complex **5** contains diamagnetic single-bonded $(C_{70}^{-})_2$ dimers that result in magnetic dilution of the paramagnetic Mn^{II} centers due to large distances between them and the pure paramagnetic behavior of **5**.

Acknowledgment. The work was partly supported by Grant-in-Aid Scientific Research from the Ministry of Education, Culture, Sports, Science and Technology, Japan (152005019, COE programs), the Russian Science Support Foundation, INTAS YSF 05-109-4653, RFBR grant no. 06-03-32824, and RFBR-JSPS grant no. 06-03-91361.

Supporting Information Available: Crystallographic data for **2**, **3**, and **5** in CIF, IR spectra data for starting compounds and **1**−**6** (Tables S1 and S2), EPR data (Table S3), UV−visible-NIR spectra of **1**−**6** and starting porphyrins (Figures S1−S4), EPR spectra of **1** and **4** (Figures S5 and S6), SQUID data for **5** and **6** (Figures S7 and S8), fitting of the molar magnetic susceptibility of **1** by Heisenberg one-dimensional antiferromagnet model (Figure S9), and EPR data for **2** (Figures S10 and S11). This material is available free of charge via the Internet at http://pubs.acs.org.

IC0611138

(28) Konarev, D. V.; Kovalevsky, A. Yu.; Khasanov, S. S.; Saito, G.; Otsuka, A.; Lyubovskaya, R. N. *Eur. J. Inorg. Chem.* **2005**, 4822.